An electromagnetic model for friction forces

John Jairo Martinez Molina

An electromagnetic model for friction forces*

John J. Martinez Molina
Univ. Grenoble Alpes, CNRS, Grenoble INP, GIPSA-Lab, 38000 Grenoble, France.
**Corresponding author Email: john.martinez@gipsa-lab.fr*

(Dated: November 21,2025)

Motivated by the fact that electromagnetic forces dominate interactions between atoms, the macroscopic behavior of velocity-dependent friction forces has been modeled by using the Steinmetz equivalent circuit, where we have included additional dissipation terms analogous to those used for including the effect of Foucault's currents in electrical machines. In this paper, friction is viewed as an energy conversion process (from mechanical to electrical). It is intended to be used for simulation, real-time estimation, and motion control design. This model is able to capture the behavior of dry friction, observed in solid surfaces in contact, and could be useful for explaining or interpreting the behavior of friction forces. This paper presents the model and includes a discussion on the conditions of model parameters for verifying the well-known Amontons-Coulomb laws of dry friction. In addition, the paper highlights three applications where the model is employed to predict various types of friction. The chosen examples are supported by experimental data and allow us to illustrate how the model can be used in other contexts.

I. INTRODUCTION

Friction is a ubiquitous phenomenon in mechanical, physical, and biological systems, playing a critical role in various aspects of daily life and industrial applications. Whether it involves braking a vehicle, designing gears, or studying intermolecular interactions, understanding and modeling friction is essential for predicting, controlling, and optimizing system performance. See for instance [1] and [2]. However, friction is also a complex phenomenon, influenced by numerous factors such as surface properties, relative velocities, normal forces, temperature, and even the microscopic scales of contact, as stated in [3] and [4], for instance.

Historically, simple models such as Amontons-Coulomb laws have been used to describe friction in practical contexts by linking it to dry contact. See [2]. While effective under limited conditions, these laws fail to capture the nuances of more complex phenomena, such as transitions between static and dynamic friction, adhesion effects, and dependencies on temperature and speed. To address these limitations, advanced models like the Dahl and LuGre models have been developed to incorporate the dynamic behavior of friction. See [5] and [6], for instance. Simultaneously, atomic-scale simulations and sophisticated numerical tools, such as finite element methods and molecular dynamics simulators, enable the study of friction at scales ranging from macrostructures to intermolecular interactions [2]. However, explainable, simple, and physical-based models for real-time estimation and motion control, are still of high interest in many applications.

The applications of friction models are numerous and diverse. They span industrial fields such as automotive (brake system optimization [7]), aerospace (contact management in composite materials [8],[9]), and additive manufacturing (control of adhesion forces [10]). Moreover, tribology—the science of friction, wear, and lubrication—extends to emerging domains like nanotechnology and biomechanics. In these contexts, a precise understanding of friction mechanisms opens opportunities to reduce energy losses, improve material durability, and design innovative systems.

In this paper we present a model inspired from physical laws of induced forces in electrical machines, very compliant with observations on triboelectricity, and the results presented in the literature that attempt to explain the **electronic mechanisms of friction**, see for instant the survey presented by J. Krim in [11], and observations presented in [12–16].

A key feature of the electrical induction machines is their ability to convert electrical energy into mechanical energy, and *viceversa*, through electromagnetic interactions between the stator and rotor. A such electromechanical conversion can be modeled by an electrical circuit, see [17]. In addition, in these machines, see [18] for instance, the induced electromagnetic torque depends nonlinearly on the slip velocity, in a similar way than that observed on tire-road interactions forces, see [4], for instance.

Thus, the **macroscopic** behavior of friction forces has been modeled as a Steinmetz equivalent circuit which includes particular dissipation terms modeling the Foucault's currents, as it is illustrated in Figure 1. Simulated examples and experimental obtained curves

* This work was partially supported by I-TireLab (2025–2029), a joint public-private laboratory focused on modeling, estimation, and control for connected tires and rubber manufacturing processes. The laboratory is supported by Michelin, Université de Poitiers, Univ. Grenoble Alpes, Grenoble INP, and CNRS.

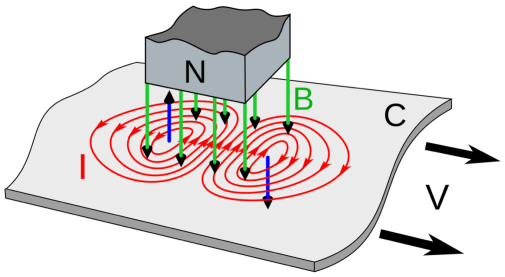

FIG. 1. An electromagnetic interpretation of induced forces of friction. The **Foucault's currents** (I) are induced within a conductive sheet (C) by the relative motion of the sheet in a magnetic field. The magnetic field, acting on the sideways moving electrons, creates a **Lorentz force** opposite to the velocity (V) of the sheet, which acts as a drag force on the sheet. Figure reprinted from [19], cc0 image licensing, 2014.

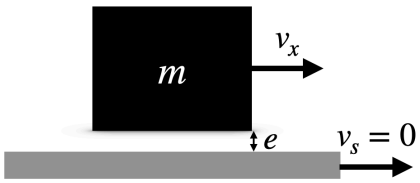

FIG. 2. An object moving with respect to a given support at speed v_x. The speed v_s can be arbitrarily fixed to zero, because here, only relative velocity (i.e. $\tilde{v} := v_s - v_x$) will be considered as the input causing friction.

are included for illustrating the effectiveness of the model for capturing well-known behaviors of friction forces. For instance, the proposed model reproduces the Stribeck effet, stiction and stick-slip, as well as, at high relative velocities, the model becomes the Coulomb model of dry friction. Compared with existing models (see for instant [6]), this model is very simple, requiring a small number of parameters to be tuned.

The proposed model concerns a new friction model which is intended for simulation, estimation and motion control design. The main features of the proposed model can be summarized as follows:

- The proposed model is able to capture the behavior of friction observed in nature, and suggests insights for respecting well-known Amontons-Coulomb laws of dry friction. In addition, the model properly fits experimental data of different types of friction (tire-road interactions, aerodynamics forces, and particles moving through matter), as it is presented in this paper.

- The model is described by a small number of parameters. Very suitable for solving **real-time** estimation and control problems. Friction is viewed as an energy conversion process (mechanical to electrical). Thus, the model parameters have physical meaning, and they are concerned with energy conversion, storage, and dissipation. These aspects are consistent with Persson's model presented in [12].

- The model can be extended for predicting friction forces in multidimensional directions. This aspect can be achieved by exploiting the geometry of the model, and without increasing the complexity of the model description.

- The model is based on physical insights of electromagnetism, in particular a model used on induction machines. Therefore, the proposed model could help us move closer to a reconciliation of friction theories, in different domains and in different scales.

The paper is organized as follows: Section II presents the preliminaries aspects concerning this work. In particular we present the motion dynamics of a system affected by friction (from a mechanical point of view), and, the proposed equivalent circuit (electrical point of view), that we will used for modeling friction. In Section III, we use the model presented in previous Section to derive the proposed friction model with a particular dissipation term. In Section IV, we extend the model to obtain a multidimensional one, by making use of the geometrical properties of the model. Section V presents illustrative simulated examples, where the model is used in different contexts, mainly related to dry friction. After that, in Section VI the conditions for which the model could be consistent with Amontons laws of dry friction is presented and discussed. Finally, in Section VII three examples for modeling different types of friction are presented. These examples are supported by experimental data, and allow us to illustrate how the model can be used in other contexts and applications. Conclusions are presented in Section VIII.

II. PRELIMINARIES

A. Motion dynamics of a system affected by friction

Consider the Newtonian dynamics of a motion system, with mass m, moving at speed v_x in the longitudinal direction x with respect to a support (our inertial frame) moving at v_s, as it is illustrated in Figure 2. Without loss of generality we can fix $v_s = 0$. The motion of the

system obeys the following dynamical equation:

$$m\dot{v}_x = F_x(\tilde{v}_x) + F_{ext} \tag{1}$$

where the friction forces has been denoted $F_x(\tilde{v})$, with $\tilde{v}$, the relative velocity, defined as:

$$\tilde{v} := v_s - v_x \tag{2}$$

Remark that, for an initial condition $v_x = 0$, the friction force appears only in presence of external forces F_{ext}, and, for a given surface conditions, the achieved magnitudes of a such friction force depend on the relative speed $\tilde{v}$. In other words, the friction force does not occur autonomously, it must be induced by other forces of motion acting on a particle of mass m, for instance.

There are no sensors capable of measuring the friction force. However we can estimate the magnitudes of friction forces from measurements of system speed v_x and external forces F_{ext} and, by using the motion dynamics (1). Predicting the friction force is more challenging since, models in the literature are complex and very difficult to tune, in particular in applications requiring real-time information of friction and its full description of the behavior for taking control decisions. In addition, the available friction models vary considerably depending on the field of application, and although attempts are being made to reconcile them, no single theory fully covers all the phenomena observed.

Here, we assume that friction forces are produced by a physical phenomenon, whose dynamics are faster than those observed from a mechanical point of view. Such a phenomenon is considered to be described by an electrical equivalent circuit, with very fast time-constant. Thus, the friction dynamics can be written, in terms of an equivalent model in steady-state.

B. Steinmetz equivalent circuit and induced forces model

In this paper we propose the use of the well-known behavior of induced forces in electrical machines for modeling friction. This is motivated by the observed induction nature of friction (i.e. friction force appears as a consequence of a relative speed). In addition, an electromagnetic model of induction machines can explicitly include the conversion mechanism due to a relative speed, energy storage terms (inductance or reactance behavior) and energy dissipation terms (electrical resistance).

Since matter contains charged particles and the relative movement of two bodies could induce Foucault's currents, as it is illustrated in Figure 1, an electromagnetic inspired model that includes Foucault's currents losses, will being a good candidate for modeling friction. In this order of ideas, we have to accept that the two surfaces (body of mass m and support) are in contact by means of an empty space (an air gap) of thickness e, as it is often accepted in contact mechanics. See for instance Lennard-Jones potential in [20], which it is often used for modeling attractive/repulsive forces at small distances between two bodies. We will show in this paper, that the electromagnetic induction model can be used for solving the friction modeling problem, providing a very simple and explainable model.

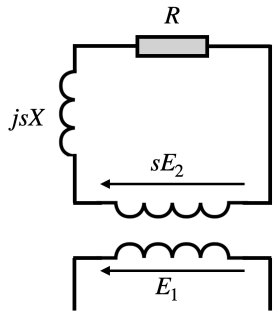

FIG. 3. Steinmetz equivalent circuit of an induction motor, representing the electromagnetic dynamics of the friction forces.

Consider the Figure 3. It represents a **Steinmetz equivalent circuit** of an induction machine. The voltage of the stator (equivalent to our support here), denoted E_1, induces a voltage on the moving component (the rotor, equivalent to our body in motion), which is proportional to the slip-ratio s. The induced voltage will be then sE_2, where the slip-ratio is defined as:

$$s := \frac{\omega_s - \omega_r}{\omega_s} \tag{3}$$

The speed ω_s corresponds to the synchronous angular speed of the stator (the inductor) and ω_r the angular speed of the rotor (the induced). This behavior can be written in terms of the following electrical equation:

$$sE_2 = (jsX + R)\, I \tag{4}$$

where X stands for the rotor reactance, R the equivalent electrical resistance, and I the induced electrical current into the rotor. Remark that at zero slip, the induced voltage sE_2 becomes zero (or equivalently, the resistance R/s becomes bigger and tends towards infinity).

We can show from (4), and by considering the dissipated power on the resistance R (i.e. **Joule heating effect**), that the induced force F_e, perceived by the rotor, can be written as follows, see for instance [18]:

$$F_e = \left(\frac{k_0 \left(\Phi_{max}\right)^2 \left(\frac{R}{X}\right)}{s^2 + \left(\frac{R}{X}\right)^2} \right) s \tag{5}$$

where k_0 is a constant that absorbs certain other parameters of the machine. Recall that the term X denotes the

equivalent reactance, function of the rotor inductance, so the equation (5) would be a steady-state description of the electrical dynamics which is considered here to be faster than the mechanical one.

For given electrical parameters, R and X, this equation can be written in terms of the "pull-out" slip, s_{max}, for which the induced force is maximum:

$$F_e = F_e(s) = \left(\frac{2\ F_{max}\ s_{max}}{s^2 + s_{max}^2} \right) \cdot s \tag{6}$$

where we have : $F_{max} = \frac{1}{2} k_0 \left(\Phi_{max}\right)^2$, and $s_{max} = \frac{R}{X}$.

This formula is known into the electrical machines domain as the **Kloss formula**, often written in terms of motor produced torque.

In addition, we can remark that, the maximum produced force F_{max} is proportional to the square of the maximum magnetic flux, Φ_{max}, and the pull out slip will be function of both R and X. We known for instance, that reducing the air gap between the stator and rotor decreases the leakage reactance X, and increases the induced voltage E_2 and by consequence increases the values of F_{max}.

Now, by considering that the magnetic flux is produced by a "constant" magnetomotive force, this magnetic flux can be written in terms of the magnetic permeance, thus, for a very small air gap thickness we have (see for instance [21]):

$$F_{max} = \frac{1}{2} k_0 \left(\Phi_{max}\right)^2 \propto \left(\frac{\mu_o S}{e} \right)^2 \tag{7}$$

where μ_o is the permeability of vacuum, S is the cross-sectional area of the air gap in square meters, and e the air gap thickness in meters.

In the next Section, we will make use of the previously presented equivalent electrical circuit, in particular equation (6), for modeling the behavior of the friction forces.

III. PROPOSED FRICTION FORCES MODEL

Consider again the motion dynamics of a mass, described by equation (1). In this paper, we propose to use the model (6) for modeling the behavior of friction forces $F_x(\tilde{v})$ in (1). In particular, we will write (6) in terms of relative velocities. That is,

$$F_x(\tilde{v}) = \left(\frac{2\ F_{max}\ \tilde{v}_{max}}{\tilde{v}^2 + \tilde{v}_{max}^2} \right) \cdot \tilde{v} \tag{8}$$

where the following relationship is used for obtaining (8) from (6):

$$\frac{\tilde{v}}{\tilde{v}_{max}} = \frac{s}{s_{max}} \tag{9}$$

since slip can be written in terms of relative "tangential" velocity, denoted $\tilde{v}$ and defined as:

$$\tilde{v} := v_s - v_x \tag{10}$$

with v_s the speed of the stator and v_x the tangential speed of the moving part of the system. Then, here $\tilde{v}_{max}$ denotes the relative tangential velocity for which the maximum force, equal to F_{max}, is achieved. Recall that v_s could be considered equal to zero, without loss of generality, since the support speed can be used as our inertial frame and it is only useful for normalizing slip velocities, as we do in equation (3) for defining slip-ratio.

For properly modeling the friction behavior, we associate to the relative velocity parameter $\tilde{v}_{max}$, the following rule:

$$\tilde{v}_{max} = \left(\tilde{v}_{max0} + \frac{1}{2} \zeta \mid \tilde{v} \mid \right) \tag{11}$$

which allows us to consider that the equivalent dissipation term (i.e. the equivalent electrical resistance), could be a function of the relative speed by means of constant parameters $\tilde{v}_{max0}$ and ζ. Thus, equation (11) allows us to include dissipation terms which model possible presence of Foucault's currents.

The proposed friction model will be thus described by equations (8) and (11). However, $\tilde{v}_{max}$ could take more complex forms according to the type of friction.

Remark that the proposed friction force (8), becomes a viscous one at small relative velocities. This is consistent with Persson's model presented in [12], as well as the increments on the resistance expressed on (11), which are compliant with observations reported in [13]. For instance, our model says that there is not friction in absence of electrical resistivity. The model proposed here could be considered as the dissipative part of the van der Waals interaction (since we consider forces dependent on relative velocity), and probably equivalent to the one presented in [22], whose hypotheses are very similar.

An interesting aspect concerns the fact that we can write the parameter $\tilde{v}_{max0}$, from (11), as:

$$\tilde{v}_{max0} = \left(1 - \frac{1}{2} \zeta \right) \lambda_{max} \tag{12}$$

where λ_{max} will be the relative velocity for which the maximum friction force is achieved, i.e. $F_x(\lambda_{max}) = F_{max}$. And by consequence, the model can be written in terms of the maximum friction F_{max}, slip at maximum friction λ_{max} and ζ. The latter, characterizes the value of the Coulomb friction, since at high relative speeds $\tilde{v}$, we have that the friction force (8) becomes:

$$F_{Coulomb} = \left(\frac{\zeta}{1 + \frac{1}{4}\zeta^2} \right) F_{max} \tag{13}$$

Remark that this model only requires to tune three parameters. It has the additional advantage that parameters have physical interpretations, concerning the storage and the dissipation of energy during the energy conversion process.

The induction of forces produced into an induction motor, could be analogous to that produced for molecular interactions, at the contact interface. In [3] for instance, it is examined how surface interactions, including Van der Waals forces, affect rubber friction. Indeed, Van der Waals forces have been widely studied to explain electrostatic adhesion between surfaces, as it is mentioned in [2].

Here, the equivalent "induction machine" model could be seen as a macroscopic model of the **velocity-dependent** intermolecular interactions forces, produced by the surfaces in contact. Remark that this model can be written in terms of the slip-ratio and/or in terms of the relative speed between surfaces.

Finally, we observe that, parameters F_{max} and λ_{max} can be related to the **Stribeck effet** observed in mechanisms affected by friction. These all aspects will be illustrated in Section V, after presenting the multi-dimensional version of the proposed model in the next Section.

IV. MULTI-DIMENSIONAL FRICTION MODEL

In this Section we extend the model for predicting friction in different directions. Very useful, for instance, in automotive dynamics for describing tire-road interactions. Here we consider the fact that longitudinal and lateral forces are components of a single vector force (i.e. the **resultant force** observed at the surface contact, for instance), and by consequence both the longitudinal and the lateral relative speeds are components of a **resultant speed vector**.

Let's define the magnitude of the resultant speed vector, as follows (by considering zero vertical speed, i.e. $\tilde{v}_z = 0$, for instance):

$$|\tilde{v}^*| = \sqrt{\tilde{v}_x^2 + \tilde{v}_y^2} \tag{14}$$

where the relative velocities in the directions x, and y, are denoted $\tilde{v}_x$, and $\tilde{v}_y$, respectively. Thus, the total force magnitude can be written as:

$$|F^*| = \sqrt{F_x^2 + F_y^2} \tag{15}$$

If we focus on the x direction for instance, remark that, geometrically, the following relationship will be respected:

$$\frac{F_x}{|F^*|} = \frac{\tilde{v}_x}{|\tilde{v}^*|} \tag{16}$$

equivalently,

$$F_x = \frac{|F^*|}{|\tilde{v}^*|} \cdot \tilde{v}_x = \mathcal{K}(\tilde{v}^*) \cdot \tilde{v}_x \tag{17}$$

Remark that (17) has the same structure than the proposed model (8), and it suggests to use this model for obtaining a more general model which includes combined motion directions.

Here, we consider the same parameters values F_{max}, $\tilde{v}_{max0}$ and ζ on all directions, however this can be different in practice and can be incorporated without difficulty to the proposed model by using techniques applied in materials science for instance, see [23]. This aspect is detailed in [24].

Now, we can write the model described by (8) and (11), in a more general form. That is,

$$F_x(\tilde{v}) = \left(\frac{2\ F_{max}\ (\tilde{v}^*_{max})}{(\tilde{v}^*)^2 + (\tilde{v}^*_{max})^2} \right) \cdot \tilde{v}_x \tag{18}$$

where,

$$\tilde{v}^*_{max} := \left(\tilde{v}_{max0} + \frac{1}{2}\ \zeta\ |\tilde{v}^*| \right) \tag{19}$$

Considering again equation (17), remark that the function $\mathcal{K}(\tilde{v}^*)$ depends on the longitudinal and lateral relative velocities, v_x and v_y. Thus, the model can be explicitly written in terms of relative velocities v_x and v_y. That is,

$$F_x(\tilde{v}_x, \tilde{v}_y) = \mathcal{K}(\tilde{v}_x, \tilde{v}_y) \cdot \tilde{v}_x \tag{20}$$

for the longitudinal friction force. By using the same geometrical arguments, the lateral forces can be written as:

$$F_y(\tilde{v}_x, \tilde{v}_y) = \mathcal{K}(\tilde{v}_x, \tilde{v}_y) \cdot \tilde{v}_y \tag{21}$$

Equations (20) and (21) are similar to those proposed in tire dynamics in [25] and [4], for modeling tire-road friction on combined slip situations. Here however, we have an explicit expression of $\mathcal{K}(\tilde{v}_x, \tilde{v}_y)$ which facilities the way to solve the multi-dimensional modeling problem.

V. ILLUSTRATIVE EXAMPLES

To illustrate the quality of the model to describe well known behaviors of friction forces, we select a number of scenarios to be simulated. In particular, we illustrate how the model reproduces the Stribeck effect, stinction and stick-slip phenomena as well as the property of the model to converge to the Coulomb friction for high relative velocities.

A. Stribeck effect and Coulomb friction

Figure 4 depicts the obtained results of simulating the proposed friction model at different relative velocities. In this scenario the model has the following parameters: $F_{max} = 1.0$, $\zeta = 0.5$ and we chose $\tilde{v}_{max0} = 0.01$ in Figure

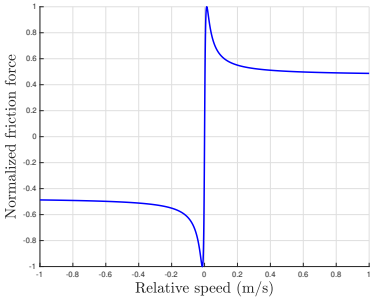

(a)

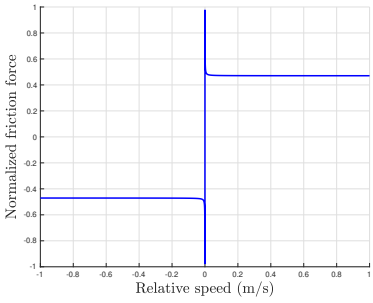

(b)

FIG. 4. Induced (normalized) friction forces, obtained by using the proposed model. Here we observe the well-known behaviors of friction forces : The Stribeck effect, the stick-slip and Coulomb friction force. Remark that Coulomb friction force seems to be independent of the relative velocity.

4(a), and $\tilde{v}_{max0} = 0.0001$ in Figure 4(b). Remark that the model is well defined at zero relative velocity, and then the curve is, in both cases, a suitable continuous curve describing friction forces. The Stribeck effect appears on cases where the parameters $\tilde{v}_{max0}$ is big enough compared to the relative velocities. The stick-slip or stiction behavior would be simply the behavior of the same phenomena but with very small values of $\tilde{v}_{max0}$ (small dissipation) compared with high values of F_{max}. Finally, we remark that parameter ζ determines the magnitude of the Coulomb friction, as a percentage of F_{max}. See equation (13).

B. Gravity-induced friction forces

Now, we consider a simulated scenario where the proposed model is used to describe the motion of a mass on an inclined plane. We select a position-based translational frame, where gravity acts downwards. Gravity induces a normal force between the mass and the plane. For this plane inclination, gravity induces positive motion along the inclined plane. We consider a slope of $\theta = 0.0873$ (5 degrees), the mass of the object $m = 0.3kg$, the initial speed of $v(0) = 1\ m/s$ (so, the relative one is $\tilde{v} = -v$). Here the friction model uses $F_{max} = 1.0$, $s_{max} = 0.01$ and $\zeta = 0.5$. The model is used into the following motion equation:

$$m\dot{v} = F_x(\tilde{v}) + mg\sin(\theta) \tag{22}$$

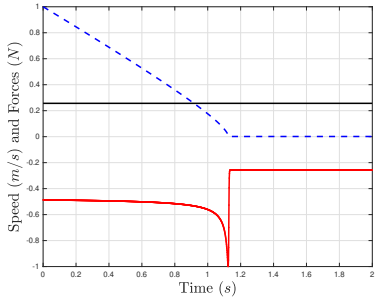

FIG. 5. Gravity-induced friction force (red curve), the gravity force (black curve) and the achieved velocity (blue dashed-line curve). Initial speed of $v(0) = 1\ m/s$ (the relative one is $\tilde{v} = -v$), the mass of the object $m = 0.3kg$, slope 5 degrees. Here the friction model uses $F_{max} = 1.0$, $\tilde{v}_{max0} = 0.01$ and $\zeta = 0.5$. We use the Euler method for simulation with sampling time of $1ms$.

and simulations are performed by using Euler method with a sampling time of $1ms$.
We observe, from Figure 22, how the velocity decreases along the time (blue dashed-line curve), due to friction forces induced by gravity (gravity force in black and friction force in red solid curve). The forces are in equilibrium once the speed is equal to zero. The friction forces converge to the Coulomb forces at high speed but, after producing a Stribeck effect just before the mass reached zero speed, the friction force converges to a constant value, equal to that produced by gravity but in opposite direction. This behavior is exactly the same described in multiple experiences on friction-affected motion dynamics.

C. Spring-mass induced friction forces

In this scenario we consider a simulated case where the proposed model is used to describe the motion of a mass attached to a spring. We select a position-based translational frame, where gravity does not affect the motion behavior. Here, we consider the mass of the object $m = 0.3kg$, a spring coefficient $k_s = 20$, the initial speed of $v(0) = 0\ m/s$ (so, the relative one is $\tilde{v} = -v$) and, the initial position $x(0) = -0.2m$ (x the current position of the mass). The proposed friction model uses $F_{max} = 1.0$, $s_{max} = 0.01$ and $\zeta = 0.5$. The friction model is used into the following motion equation:

$$m\dot{v} = F_x(\tilde{v}) + k_s x \tag{23}$$

$$\dot{x} = v \tag{24}$$

and simulations are performed by using Euler method with a sampling time of $1ms$.

From Figure 6, we observe how the velocity oscillates along the time (blue dashed-line curve), due to friction forces induced by the spring response (spring force in

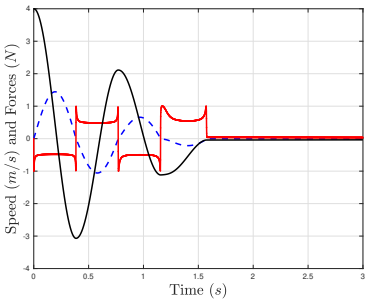

FIG. 6. A spring attaches a mass of $m = 0.3kg$ to a stationary wall. At time = 0 seconds, initial targets for the spring (spring coefficient equal to 20) put it in a state of compression under a 4 N load. Initial speed of $v(0) = 0\ m/s$, (the relative one is $\tilde{v} = -v$), initial position $x(0) = -0.2\ m$. Here, we observe the spring-induced friction force (red curve), the spring force (black curve) and the achieved velocity (blue dashed-line curve). Here the friction model uses $F_{max} = 1.0$, $\tilde{v}_{max0} = 0.01$ and $\zeta = 0.5$.We use the Euler method for simulation with sampling time of $1ms$.

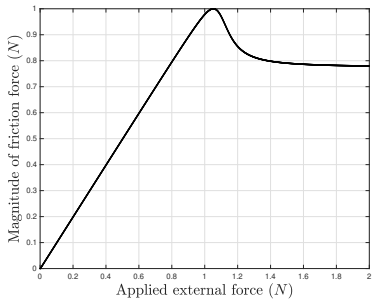

FIG. 7. Induced (normalized) friction forces predicted by the proposed model with respect to applied external force (increasing on ramp). We observe the static region, for less than $1N$ and the kinetic region, for more than $1N$ of applied force. The Coulomb friction appears for very big external forces, in the kinetic region. Remark that Coulomb friction seems to be independent of relative velocity. The proposed friction model uses $F_{max} = 1.0$, $\tilde{v}_{max0} = 0.01$ and $\zeta = 0.95$.

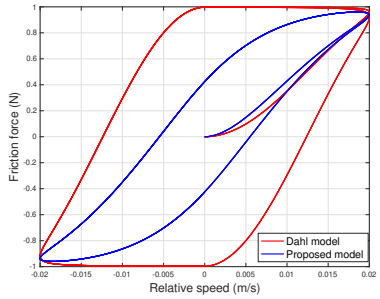

FIG. 8. Hysteresis effect: Dahl model *vs.* proposed model.

black and friction force in red solid curve). The forces are in equilibrium once the speed is equal to zero. The friction forces cross the Coulomb forces at high speed but, after producing a Stribeck effect just before or after the mass reached zero speed. At the equilibrium, the friction force converges to a constant value, equal to that produced by the spring but in opposite direction. This behavior is exactly the same described in multiple experiences on friction-affected spring-mass system motion dynamics.

D. Static and kinetic regions of friction forces

In this example, we simulate an object of mass m affected by an external force producing a motion which obeys (1). The external force F_{ext} increases linearly with respect to time. Figure 7 illustrates the obtained induced friction force, predicted by the proposed model, with respect to the applied external force. We observe the static region for less than $1N$ (i.e. with linear increments of friction), and, the kinetic region, for more than $1N$ of applied force (where friction seems to be in saturation). The Coulomb friction appears for very big external forces, in the kinetic region. Remark that Coulomb friction seems to be independent of relative velocity. The proposed friction model uses $F_{max} = 1.0$, $\tilde{v}_{max0} = 0.01$ and $\zeta = 0.95$, and it behaves as expected in mechanisms affected by friction.

E. Hysteresis and Pre-sliding displacement

If we use a dynamical version of the proposed model, it is possible to observe a hysteresis effect, as stated in the literature for very small displacements.

The dynamical model can be written, by using Euler method, as

$$F_x^+ = \alpha F_x + (1-\alpha)\left(\frac{2\ F_{max}\ \tilde{v}_{max}}{\tilde{v}^2 + \tilde{v}_{max}^2}\right)\cdot \tilde{v} \qquad (25)$$

where F_x^+ stand for the friction force at the new time instant, and α a constant which depends on a given sampling time. The parameter α will allow us to add a dynamical behavior of friction, as it is made on induction forces in electrical machines. See for instance [18].

Dahl's model is widely used to represent hysteretic friction at micron-scale displacements, which resembles stress-strain curves for solid materials. Hysteretic friction refers to the time-history dependence of friction in the pre-sliding regime which arises due to microscopic sliping of the surface asperities. This type of friction can be visualized as the stretching of 'soft springs' between surfaces in relative motion; the springs are linearly elastic at small micro-displacements and yield plastically at larger displacements. Here, the proposed model (25) has an additional degree of freedom for capturing hysteresis, since the parameter α can be used for modeling a time constant of the electrical dynamics and then obtaining

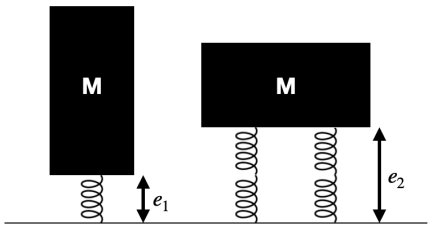

FIG. 9. Air gap for different contact surfaces. Here, two blocks of mass M has a contact surface, equal to S_1 for the first one (left hand) whereas the second one has a contact surface equal to $S_2 = 2S_1$ (right hand). The air gap due to weight will be different and, $e_2 = 2e_1$ if we assume a linear spring behavior between contact surfaces.

different shapes of those curves. A full electromagnetic induction forces model, as that used in induction machines modeling, see for instance [18], could provide more accurate results during the transient evolution of friction. However, these detailed models often require more computational resources. So, the dynamical model (25) provides an interesting trade-off between model complexity and desired accuracy for describing the friction phenomena, and by consequence it could be very useful for system simulation, state estimation and motion control.

VI. CONDITIONS FOR RESPECTING AMONTONS' LAWS OF DRY FRICTION

Consider the well known laws of dry friction stated by Amontons. That is,

1. Friction is proportional to the force that presses the surfaces together. That is, for a given "normal load" F_N, we have: $F_x \propto F_N$.

2. The second law states that friction force is independent of the apparent area of contact.

3. A third law, attributed to French physicist Charles Augustin Coulomb, is frequently included with those of Amontons: The friction force is independent of velocity for ordinary sliding speeds. That is,

$$\lim_{\tilde{v}\to\infty} F_x(\tilde{v}) = F_{Coulomb} \tag{26}$$

for a constant $F_{Coulomb}$.

Consider now the expression (7) for a given (constant) contact surface S. We remark that the proposed model can be consistent with the **first Amontons law**, if the parameter F_{max} verifies:

$$F_{max} \propto F_N \tag{27}$$

That is, the term $(1/e)^2$ in (7) will vary "approximately" linearly with respect to the normal force F_N. This is true for very small values of air gap e. This proportional relationship, presented in equation (27), is consistent as well with models adopted in contact mechanics and tire-road interaction modeling. So the model is consistent with the macroscopic response of the system to changes in load, reported by Bowden and Tabor [26]. However, The friction analysis of Bowden and Tabor does not reveal the physical mechanisms that underlie frictional energy dissipation.

In addition, if friction force is independent of the apparent area of contact (**second Amontons law**), this means that in our model (see parameter F_{max} in (7)), for two blocks of mass M in contact with the floor with different contact surfaces verifying $S_1 < S_2$, the following relationship will be met:

$$F_{max} \propto \left(\frac{\mu_o S_1}{e_1}\right)^2 = \left(\frac{\mu_o S_2}{e_2}\right)^2 \tag{28}$$

if the air gaps verify $e_1 < e_2$ in the same proportion.

This aspect is illustrated in Figure 9, where we consider that the surfaces are $S_2 = 2S_1$. So, since the forces can be considered to be homogeneously distributed in the surfaces, the air gap e_2 will be more bigger than e_1, and $e_2 = 2e_1$. This behavior can also be explained by considering, in the normal direction, that the two surfaces in contact obey the Hooke's law (as we often do in contact mechanics, see [20]), and then, the second Amontons law will be respected by the proposed model.

Finally, the **third law of dry friction** is naturally respected by the proposed model, since the model converges to a Coulomb friction at high relative velocities, and its value will be function of parameters F_{max} and ζ, by means of relation (13). This aspect has been previously illustrated in Figure 4.

VII. EXAMPLES OF MODELING DIFFERENT TYPES OF FRICTION BY USING THE SAME PROPOSED MODEL

Today, we already known that **droplet friction** found to be similar to that of solid objects. See [27], for instance. So, the proposed model could be suitable for predicting friction on different kind of surfaces. Here we illustrate how the model fits properly to experimental data in cases where the observed friction is dominated by visco-elastic/solid interactions, as well as for air/solid interactions. In addition, we illustrate a possible use of the model for computing a Bragg curve in radiation applications, where protons loss kinetic energy during its travel through matter.

A. Tire-road interaction friction modeling

In this example we consider the behavior of friction forces at tire-road contact level. Here we treat the tire as a body that is in contact with the road and subject to slip. Here, the symbol s_x stands for the tire slip-ratio, for both traction or braking situations, and defined as:

$$s_x := \frac{\omega r_w - v_x}{v_x} \tag{29}$$

where ω stands for the angular velocity of the wheel, r_w stands for the effective radius of the corresponding free-rolling tire. The lateral slip s_y will be defined as:

$$s_y := \frac{-v_y}{v_x} \tag{30}$$

The symbols v_x and v_y stand for the longitudinal and the lateral velocities (measured at the center of the contact patch), respectively.

Since in automotive applications, the slip-ratios are often used for describing the level of tire-road adherence, the proposed model (6) is used for deriving the following model of tire-road interaction friction force. Thus, in the longitudinal direction, we have:

$$F_x(s_x) = \left(\frac{2\ F_{max}\ s_{max}}{s_x^2 + s_{max}^2} \right) \cdot s_x \tag{31}$$

where

$$s_{max} = \left(s_{max0} + \frac{1}{2}\zeta \mid s_x \mid \right) \tag{32}$$

with constant parameters F_{max}, s_{max0}, and ζ.

The model predicts the contact friction forces with similar accuracy than those achieved by the Pacejka Magic Formula, one of the most used model for tire-road interaction in automotive industry, see [4]. Here however, by using only three parameters, we achieve more than 98.9% of model FIT (computed as R^2 in percentage). An experimental validation of the proposed model for tire-road interaction modeling, using data from a flat track tire testing machine, is presented in [24]. For instance, Figure 10 illustrates the behavior of the pure longitudinal tire-road friction with respect to the longitudinal slip, and it is compared to that obtained by using the proposed model. The model parameters have been obtained by solving a nonlinear optimization problem, achieving more than 93% of model FIT. In [24], the application of the model in its multi-dimensional form, is also presented. The experiences presented in [24], show that the model is able to capture the complex behavior of tire-road interactions by including a possible anisotropy of the model parameters. Thus, the model parameters can take values according to the slip direction, as we do for modeling anisotropic properties in materials science for instance, see [23].

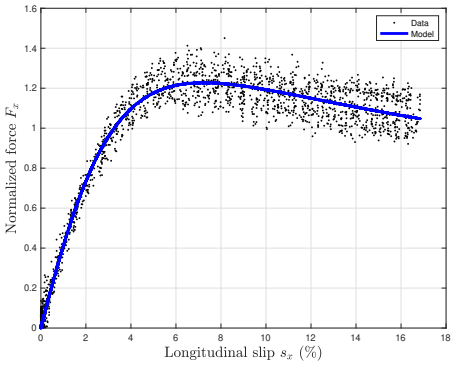

FIG. 10. Longitudinal normalized friction forces with respect to longitudinal slip. Here we are fixing the parameters of the model as $F_{max} = 1.227$, $s_{max0} = 5.55$ and $\zeta = 0.46$, for a neglected lateral slip scenario, i.e. $s_y \approx 0$. Normalized with a normal force around $3500N$. The obtained FIT, with respect to experimental data, is equal to 93.01%. Figure reprinted from [24].

Figure 12 illustrates the obtained prediction on longitudinal and lateral forces by using the proposed model with available slip-ratios s_x and s_y, presented in Figure 11. We can observe the behavior of friction forces with respect to the simultaneous lateral and longitudinal slips. The proposed model capture this aspect with high accuracy. Using the multi-dimensional model version, presented in Section IV, we have computed the longitudinal forces as:

$$F_x(s_x, s_y) = \mathcal{K}(s_x, s_y) \cdot s_x \tag{33}$$

whereas the lateral forces, are computed as:

$$F_y(s_x, s_y) = \mathcal{K}(s_x, s_y) \cdot s_y \tag{34}$$

Remark that **the stiffness** $\mathcal{K}(s_x, s_y)$, as it is called in the automotive domain, is shared for both longitudinal and lateral interactions forces. Keeping the simplicity of the model for using in combined slip situations.

B. Aerodynamic forces modeling

The lift coefficient in aerodynamics applications are obtained by normalizing the lift forces by:

$$F_N = \frac{1}{2}\rho S \tilde{v}_x^2 \tag{35}$$

The force F_N can be considered to be the force that presses the air to the surface of the airfoil. The parameter ρ concerns the air density, S the surface in contact, and $\tilde{v}_x$ the relative velocity of the air with respect to the airfoil. Here we consider $\tilde{v}_x = -v$, with v the wind speed magnitude (since we use data from a wind tunnel test series, where the airfoil speed is zero, and the airflow speed

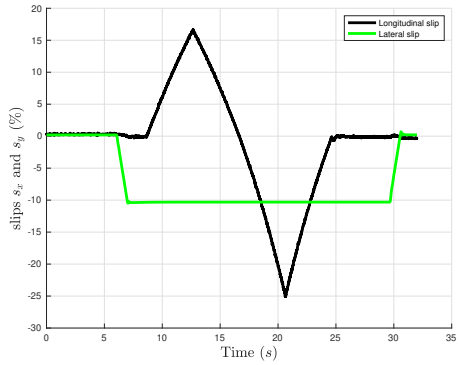

FIG. 11. Measurements of longitudinal and lateral slips (in percentage), during a combined slip situation. Figure reprinted from [24].

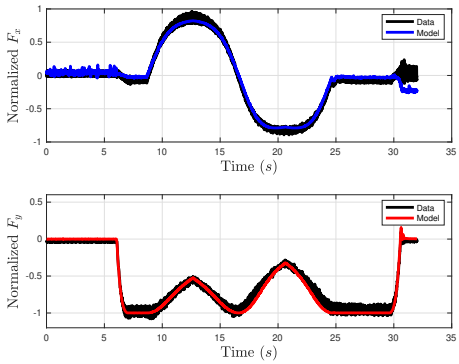

FIG. 12. Longitudinal and lateral forces, measured and predicted ones from model with respect to time. Normalized with a normal force around $4500N$. The obtained FIT is more than 92%. Figure reprinted from [24].

v_x will be $v_x \approx v$, for small angles of attack). Data has been obtained from [28], and it concerns a NACA 0012 airfoil (a symmetrical airfoil) at different angles of attack, and subject to a wind speed with different Reynolds number.

The slip ratio, similar to that defined in previous example, will be obtained from the angle of attack, denoted α. Since for small angles of attack, we have:

$$\alpha \approx \tan(\alpha) = \frac{-v_z}{v_x} \tag{36}$$

where v_z stands for the vertical component of wind speed vector v (due to angle of attack α). Thus, the proposed model suggests that the lift force is produced as a reaction of v_z, and then we can write the lift coefficient (or the lift force) in terms of the angle of attack α. That is,

$$C_L(s) = \left(\frac{2\ C_{max}\ \alpha_{max}}{\alpha^2 + \alpha_{max}^2} \right) \cdot \alpha \tag{37}$$

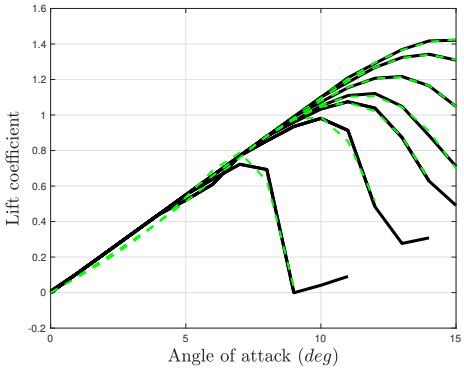

FIG. 13. Lift coefficient with respect to angle of attack for different Reynolds number. Solid dark lines concerns data and green dashed lines concerns the proposed model. Here, data have been obtained from [28].

where α_{max} obeys the following rule:

$$\alpha_{max} = \left(\alpha_{max0} + \frac{1}{2}\zeta_1 \mid \alpha \mid + \frac{1}{2}\zeta_2 \mid \alpha \mid^2 \right) \tag{38}$$

We have chosen a such function α_{max} to fit experimental data. Remark that the model requires an additional parameter ζ_2 multiplying the square of α. This term compensates the absence of data concerning relative speed on the direction x and can be interpreted as a decrease on the dissipation term.

Here we obtain for instance, values of model parameters equal to $C_{max} = 1.42$, $\alpha_{max0} = 25.38$, $\zeta_1 = 0.50$ and $\zeta_2 = -0.135$, for a Reynolds number $Re = 1000e4$. The latter parameter is negative and we remark that the value of α_{max} remains positive but decreases as α increases. The achieved model FIT in this example was 99.7%, that suggests that the proposed model is consistent with the modeled phenomena and it could be useful for characterizing the aerodynamics of a given airfoil.

Figure 13 illustrates the achieved lift coefficients at moderated values of angle of attacks for different Reynolds number: $Re = 1000e4$, $500e4$, $200e4$, $100e4$, $70e4$, $36e4$ and $8e4$. . Data is plotted in solid dark lines, whereas the model is plotted in green dashed lines. The achieved model FITs is more than 99%, by taking data from zero to critical angle of attack (when airfoil stalls). Thus, a simple model of friction can be used for interpreting and modeling the behavior of airfoils dynamics. We imagine that it could be improved if slip velocities are available in all directions.

C. Modeling a charged particle moving through matter

Here we consider the behavior of protons moving through matter. The Bragg peak is a pronounced peak on the Bragg curve which plots the energy loss of ionizing radiation during its travel through matter, see [29].

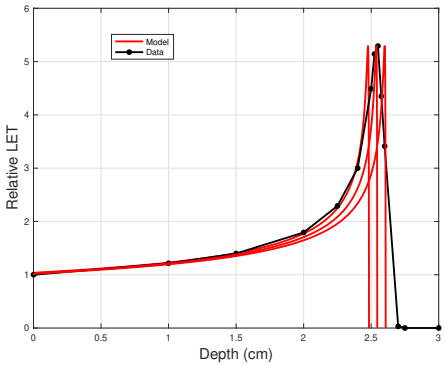

FIG. 14. A typical Bragg curve, concerning experimental data of 55 MeV Protons (The LET at the entrance point is 1.162 $keV/\mu m$ in water). Used data is plotted in black dotted lines. Here we use the proposed model with $F_{max} = 5.291$, $v_{max0} = 0.0115$ (m/s) and $\zeta = 0.005$ for different initial speeds: $v(0) = 12 \pm 0.1$ cm/s and normalized particle mass. The curves concerning the model are plotted in solid red lines. The peak would be equivalent to peak produced by the Stribeck effect in dry friction. Different initial speeds produce a spread out Bragg peak, which is useful in modern radiation therapy, for instance.

The proposed model could be used for improve radiation technologies since the break distance could be estimated from an analytic expression of motion, proposed in this paper. In this example, the model has been simulated in a similar way that that presented as an example of system motion in Section V C. Particularly, the speed and the displacement of a given particle have been computed by using the following motion equations:

$$m\dot{v} = F_x(\tilde{v}) \tag{39}$$

$$\dot{x} = v \tag{40}$$

where x, initialized at $x(0) = 0$, will be the distance traveled by the particle, whereas v, will be the speed of a such particle, initialized with the speed at the entrance point $v(0) \neq 0$. Without loss of generality, the mass m of the particle has been normalized since the force F_x (i.e. the force acting on the charged particle), can absorbs its value according to the chosen units. For instance, F_x is often measured in MeV/cm (i.e. a force, even if, in this context, this force is also called the Stopping power), but it could be sometimes associated to energy loss per kilogram of matter (Gray units), for measuring the delivered dose in radiotherapy, for instance.

Figure 14 illustrates the behavior of Bragg curves for a 55 MeV protons, where the LET (a unit of force) at the entrance point is 1.162 $keV/\mu m$ in water. Used experimental data is plotted in black dotted lines (data obtained from [30]). Here we use the proposed model with $F_{max} = 5.291$, $v_{max0} = 0.0115$ (m/s) and $\zeta = 0.005$ for different initial speed: $v(0) = 12 \pm 0.1$ cm/s and normalized particle mass. The curves concerning the model are plotted in solid red lines.

We can observe in this Figure, that the proposed model could be useful for predicting the achieved spread out Bragg peak (SOBP), due to small variations on the initial proton speed, which allows, for instance, the treatment of larger tumors, as proposed in [31]. So, future work in this area, could consider the multi-dimensional friction model presented in Section IV for improving, for instance, the achieved trajectories in more dimensions.

VIII. CONCLUSIONS

In this paper, we have proposed a friction model which is able to describe the macroscopic behavior of friction forces on motion dynamics. The model reproduces the Stribeck effet, stiction, stick-slip, and, for high relative speeds, the model converges to the Coulomb friction model. Simulated scenarios of friction are presented to illustrate the performance of the model to capture the behavior of friction forces in different contexts. In addition, we have illustrated the ability of the model to describe friction in different real situations. Conditions for which the laws of dry friction can be verified by the model, has also been presented.

The proposed model concerns a physical-inspired model, useful for describing friction in different contexts and in different scales. The friction behavior has been modeled from an equivalent electrical circuit, used for modeling induction machines. So, friction is viewed as an energy conversion process (mechanical to electrical), where conversion, storage and dissipation terms appear explicitly in the model formulation.

IX. ACKNOWLEDGEMENTS

Author would like to thank: Pierre Susbielle and Jonathan Dumon (GIPSA-lab, France), Thibault Dairay and Maxime Boulanger (Michelin, France), for their helpful feedback and scientific discussions.

[1] K. J. Astrom and C. Canudas de Wit, Friction models and friction compensation, European Journal of Control **1**, 235 (1995).

[2] J. Krim, Resource letter: Fmmls-1: Friction at macroscopic and microscopic length scales, American Journal of Physics **70**, 890 (2002).

[3] B. N. J. Persson, Theory of rubber friction and contact mechanics, Journal of Chemical Physics **115**, 3840 (2001).

[4] H. B. Pacejka, *Tire and Vehicle Dynamics*, 2nd ed. (Butterworth-Heinemann, Oxford, UK, 2006).

[5] C. Canudas de Wit, H. Olsson, K. J. Astrom, and P. Lischinsky, A new model for control of systems with friction, IEEE Transactions on automatic control **40**, 419 (1995).

[6] C. Canudas de Wit, P. Tsiotras, E. Velenis, M. Basset, and G. Gissinger, Dynamic friction models for road/tire longitudinal interaction, Vehicle System Dynamics **39**, 189 (2003).

[7] J. J. Martinez and C. Canudas de Wit, A safe longitudinal control for adaptive cruise control and stop-and-go scenarios, IEEE Transactions on Control Systems Technology **15**, 246 (2007).

[8] J. R. Hutchinson and M. D. Thouless, Contact mechanics and adhesion in aerospace composite materials: Implications for design and maintenance, Journal of Applied Mechanics **87**, 031002 (2020).

[9] A. Cappadonia and R. Kumar, Tribological behavior of aerospace composites: Friction and wear analysis, Tribology International **120**, 120 (2018).

[10] M. Schmid, A. Amado, and K. Wegener, Friction and adhesion in additive manufacturing: Implications for layer bonding and surface finish, Additive Manufacturing **7**, 25 (2015).

[11] J. Krim, Friction and energy dissipation mechanisms in adsorbed molecules and molecularly thin films, Advances in Physics **61**, 155 (2012).

[12] B. Persson, Surface resistivity and vibrational damping in adsorbed layers, Physical Review B **44**, 3277 (1991).

[13] A. Dayo, W. Alnasrallah, and J. Krim, Superconductivity-dependent sliding friction, Physical Review Letters **80**, 1690 (1998).

[14] V. Popov, Electronic contribution to sliding friction in normal and superconducting states, Journal of Experimental and Theoretical Physics Letters **69**, 558 (1999).

[15] J. Krim, Controlling friction with external electric or magnetic fields: 25 examples, Frontiers in Mechanical Engineering **5**, 22 (2019).

[16] K. P. Olson and L. D. Marks, What puts the "tribo" in triboelectricity?, Nano Letters **24**, 12299 (2024).

[17] C. P. Steinmetz, The alternating current induction motor, Transactions of the American Institute of Electrical Engineers **XIV**, 183 (1897).

[18] W. Leonhard, *Control of Electrical Drives*, 3rd ed. (Springer, Berlin, Germany, 2001).

[19] Chetvorno, Eddy currents due to magnet - cc0 image licensing (2014).

[20] V. L. Popov *et al.*, *Contact mechanics and friction* (Springer, 2010).

[21] A. E. Fitzgerald, C. Kingsley, and S. D. Umans, *Electric Machinery*, 6th ed. (McGraw-Hill, New York, 2003).

[22] A. Volokitin and B. Persson, Theory of friction: Contribution from fluctuating electromagnetic field, Physics of Low-Dimensional Structures (PLDS) **1998**, 17 (1998).

[23] V. Diana and V. Carvelli, A continuum-molecular model for anisotropic electrically conductive materials, International Journal of Mechanical Sciences **211**, 106759 (2021).

[24] J. J. Martinez, M. Boulanger, O. Sename, T. Dairay, and J. Vayssettes, A new tire-road interaction friction model for vehicle dynamics applications, Submitted to IFAC World Congress (2025).

[25] E. Bakker, L. Nyborg, and H. B. Pacejka, Tyre modelling for use in vehicle dynamics studies, SAE Technical Paper Series (1987).

[26] F. P. Bowden and D. Tabor, *Friction and Lubrication of Solids, vol. 2* (Clarendon press, 1964).

[27] N. Gao, F. Geyer, D. W. Pilat, S. Wooh, D. Vollmer, H.-J. Butt, and R. Berger, How drops start sliding over solid surfaces, Nature Physics **14**, 191 (2018).

[28] R. E. Sheldahl and P. C. Klimas, *Aerodynamic characteristics of seven symmetrical airfoil sections through 180-degree angle of attack for use in aerodynamic analysis of vertical axis wind turbines*, Tech. Rep. (Sandia National Lab.(SNL-NM), Albuquerque, NM, United States, 1981).

[29] K. Lapen and Y. Yamada, The development of modern radiation therapy, Current Physical Medicine and Rehabilitation Reports **11**, 131 (2023).

[30] NSRL, Bragg curves and peaks, NSRL User Guide - Brookhaven National Laboratory (2023).

[31] D. Jette and W. Chen, Creating a spread-out bragg peak in proton beams, Physics in Medicine & Biology **56**, N131 (2011).